

# A BiCMOS Ultra-Wideband 3.1-10.6GHz Front-End

Fred S. Lee and Anantha P. Chandrakasan

Department of Electrical Engineering and Computer Science  
MIT Microsystems Technology Laboratory, Cambridge, MA, 02139, USA

## Abstract

A direct-conversion receiver for 500MHz-wide FCC-compliant UWB pulses in the 3.1-10.6GHz licensed band is fabricated using 0.18 $\mu$ m SiGe BiCMOS. The packaged chip consists of a wideband LNA, filter, phase-splitter, 802.11a switch-able notch filter, 3.1-10.6GHz LO amplifiers, mixers, and baseband channel-select filters/buffers. The average conversion gain, NF and input P1dB are 32dB, 4dB, and -41dBm respectively. The chip draws 30mA from 1.8V. Wireless testing of the receiver at 100Mbps reveals a  $2.7 \times 10^{-3}$  bit-error-rate at -81dBm sensitivity.

## Introduction

Ultra-wideband (UWB) wireless signals were recently approved by the FCC to operate in the 3.1-10.6GHz band at a low EIRP of -41.3dBm/MHz with a minimum signal bandwidth of 500MHz [1]. The IEEE 802.15.3a task group is targeting UWB radios to provide wireless data transfer of up to 480Mbps and 1.32Gbps at short range [2].

Though UWB signals do not contribute significant interference to narrowband systems, the reverse is not true, as narrowband interferers can easily saturate a UWB front-end. Mitigating wideband noise and accounting for RF package and bond wire effects add complexity to the integration process.

This paper describes the design and measurement of an RFIC UWB front-end direct-conversion receiver *packaged* in a QFN housing that demonstrates a  $2.7 \times 10^{-3}$  bit-error-rate (BER) at a -81dBm receiver sensitivity while consuming only 50mW. These metrics are achievable due to the system architecture and an LNA that is optimized for low noise figure (NF) without requiring power match [3]. The chip also features a single-to-differential converter with an embedded notch filter for rejecting known narrowband interferers. The chip is fabricated in 0.18 $\mu$ m 60GHz $f_i$  SiGe BiCMOS.

## System Architecture

A diagram of the receiver system that incorporates this RF front-end is shown in Fig. 1. Based on system analysis and simulation, 4dB of NF is budgeted for the front-end to allow the receiver to achieve a BER of  $10^{-5}$  in the lower sub-bands at 10m. A maximum fixed gain of 38dB is sufficient to handle the signals listed in Table 1 while interfacing to a 500MS/s ADC whose full-scale input amplitude is 250mV.

The RFIC designed in this work has a similar architecture to [4]. It is comprised of a single-ended LNA followed by an integrated 2<sup>nd</sup>-order high-pass filter for improved out-of-band interference rejection at minimal cost to NF. This is followed by an RF single-to-differential converter with a switch-able notch filter to suppress unwanted 802.11a signals. The phase

splitting done after the 1<sup>st</sup> stage LNA helps to maintain low system NF and allows the RF notch filters to be easily implemented. The mixers are degenerated double-balanced Gilbert cell mixers. The local oscillator (LO) for the mixers is generated externally. The baseband output is filtered, buffered, and interfaced to the remaining receiver chain via AC-coupling to suppress  $1/f$  noise and DC offsets.

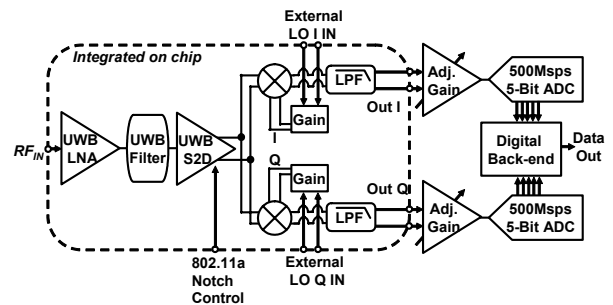


Figure 1. Block diagram of UWB direct-conversion receiver

TABLE 1 – Extremes of input signals to receiver [5]

Signals	Power @ TX	TX-RX Distance	Power @ RX	V <sub>ampl</sub> @ RX
500MHz UWB @ 3.35GHz	-14dBm	30cm	-47dBm	2.6mV
500MHz UWB @ 10.35GHz	-14dBm	10m	-87dBm	26 $\mu$ V
802.11a @ 5.25GHz	15 dBm	1m	-29dBm	10mV
Random @ 3.1GHz	0 dBm	1m	-39dBm	3.2mV

## Circuit Design

### A. Low-Noise Amplifier

Though narrowband inductively-degenerated cascode LNAs can be extended to provide a good input match and low NF for UWB LNAs, the input match becomes difficult to maintain if the circuit is bonded to a PCB or a package. The down bond(s) that form the emitter degeneration also limit the achievable  $NF_{min}$ . This problem exists because the  $NF_{min}$  at frequency  $f$  for a cascode LNA is proportional to  $fff_i$ . To achieve a match, it is necessary to bias the cascode LNA at a lower  $f_i$  because of the relatively large degeneration inductor of the package. A fully differential LNA would allow smaller on-chip degeneration inductors to be realized and thus achieve better NF and input match, but differential RF signals spanning a decade in frequency are difficult to obtain. Thus, full-band UWB LNAs are limited to single-ended topologies.

The UWB LNA here does not attempt to achieve impedance match. Instead, the LNA is viewed as a voltage amplifier and designed such that the NF to a 50 ohm source is minimized at

10GHz. Because an input match is not required,  $Q_1$  in Fig. 2 can be biased at a high  $f_i$  for low-noise performance with minimum current. To suppress reflections due to an unmatched LNA, the antenna must be placed close to the LNA to reduce transmission line effects. The nearness of the antenna to the IC is desirable for minimizing cable losses that directly impact system NF. An electromagnetic simulator is used to verify the antenna response to unmatched loads.

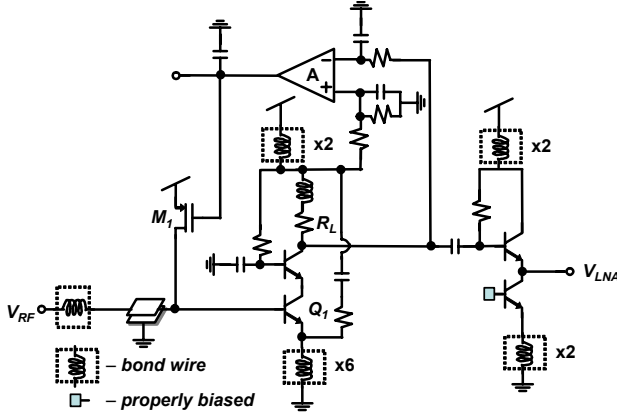


Figure 2. Low-noise amplifier and buffer

The UWB LNA in Fig. 2 is biased with a high-impedance PMOS drain  $M_1$  embedded in a microwatt feedback loop that monitors collector current through  $R_L$  and sets  $g_m$  of  $Q_1$  while contributing minimal noise. The buffer is optimized to interface the LNA to the high-pass filter and active splitter.

### B. Channel-Select Filter and Single-to-Differential Converter

The channel select filter shown in Fig. 3 is formed by a three element high-pass ladder network with two capacitors and shunt inductor. The low-pass portion of the channel select filter is formed by the cascaded amplifier roll-off.

The single-to-differential converter has a cross-coupled low-frequency PMOS loop that equalizes current differences between the differential pairs to ensure balanced operation.

The switch-able notch filter uses parallel  $LC_1$  and  $LC_2$  resonances that degenerate the emitters of the differential pair transistors with a high-impedance at their respective resonances. This reduces the gain at those frequencies. The notch frequencies are fixed at  $1/\sqrt{LC}$ . Any combination of LC is possible to create the filter. However, smaller parasitic series resistances are obtainable with smaller inductors, thus producing a sharper notch filter characteristic. The notch frequencies of both LC structures are centered at 5.25GHz and 5.75GHz, where 802.11a signals may appear. The switch to bypass the notch filters is AC-coupled to the emitters of the differential amplifier transistor pair. This allows the switch to be reasonably sized while still having a low on-resistance because of the large overdrive. The notching and phase-splitting are done after the LNA so that overall system NF is not significantly degraded.

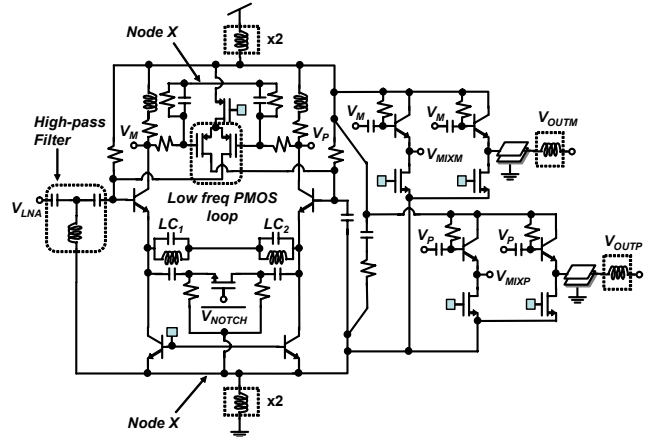


Figure 3. Channel-select filter and single-to-differential converter

### C. Mixers and LO Amplifier Chain

The mixers are conventional double-balanced Gilbert mixers. The RF input is degenerated to increase dynamic range (DR) and linearity while decreasing the load on the previous stage. A 250MHz 1<sup>st</sup>-order low-pass filter is implemented at the output for attenuating high frequency mixing products. Higher order filtering is desired for further channel-selection. The AC-coupling capacitors are off-chip.

The LO gain stages convert single-ended signals to differential and refine the signal through a cascade of two differential amplifiers with low common-mode gain. On-chip amplification of the LO is useful for reducing the external bond wire coupling of LO-RF and LO-LO signals.

## Measured Results

To verify the RFIC front-end functionality, measurements on the packaged chip are completed and reported in Section A. To verify the front-end in a wireless system environment, Fig. 1 is constructed and measurements are reported in Section B.

### A. Non-Wireless RFIC Measurements

The receiver conversion gain and NF shown in Fig. 4 are measured by sweeping the RF input from 3.1-10.6GHz and offsetting the LO frequency by 50MHz so that a baseband signal at 50MHz is observed.

The average conversion gain is 32dB and varies +/-5dB across the bandwidth. The chip was originally designed for testing in a chip-on-board system but is packaged for robustness. The larger parasitic capacitances of the package (500fF) and bond wire/pin inductances (2nH) impact the RF passband. However, a system NF from 3.3dB to 5dB (4dB average) is still achieved across the 3.1-10.6GHz bandwidth. Therefore, a flat conversion gain curve can conceivably be recovered by baseband gain compensation without degrading NF significantly. The input P1dB increases from -46dBm at 3.1GHz to -36dBm at 10.6GHz.

When the notch filter is activated, the attenuation is 10dB. The frequency of the notch filter is off due to over-accounted parasitics, but functionality of an RF notch in a UWB receiver

system can still be examined. This filter allows the receiver to tolerate an additional 10dB of interferer power within the notch frequencies.

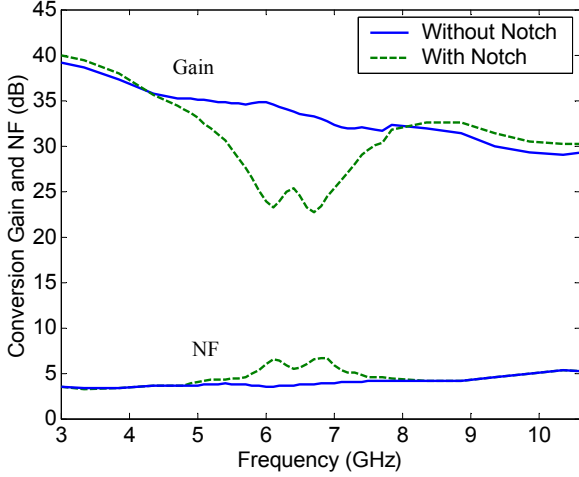


Figure 4. Measured conversion gain and NF

The effectiveness of the notch filter is shown in Fig. 5. A 3.35GHz UWB pulse is down-converted in the presence of a 6.75GHz narrowband interferer at increasing power levels. The front-end and conversion gain suffer from gain compression due to the interferer. However, when the filter is functional, the gain can be recovered up to 6.5dB.

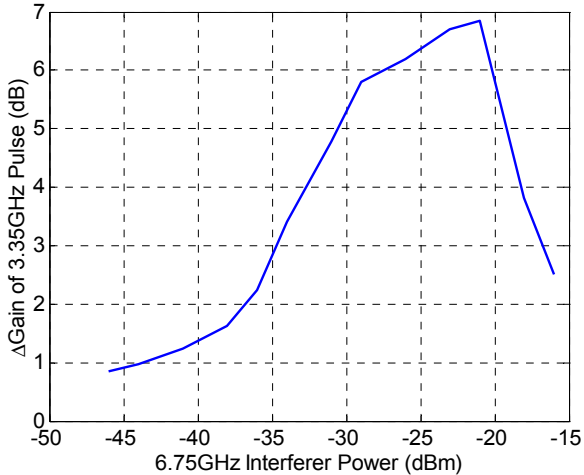


Figure 5. Notch filter effectiveness for increasing immunity to interferers

### B. Wireless System Measurements

To verify the un-matched RFIC in a wireless environment where reflections may exist, a setup using a horn antenna for wireless transmission, UWB antenna [6] for reception, and the front-end is assembled. Max/min gain excursions at the load due to reflections occurring in a transmission line with both ends un-matched are theoretically described by (1) and (2), where  $L$  is loss in the transmission line [7].

$$A_{\max} = (1 - L^2 |S_{11, \text{Antenna}}| |S_{11, \text{LNA}}|)^{-1} \quad (1)$$

$$A_{\min} = (1 + L^2 |S_{11, \text{Antenna}}| |S_{11, \text{LNA}}|)^{-1} \quad (2)$$

Fig. 6a is a plot of normalized conversion gain. The reference plot is generated by piecing together the channel loss from the TX to RX antenna and the RFIC conversion gain. Both measurements are done in reflection-less environments by ensuring at least one end of the transmission line used in each measurement is properly terminated. The total transfer gain is obtained by directly measuring the conversion gain between the TX and RX antenna/RFIC baseband output, and is subject to reflections occurring in the short transmission line between the antenna and front-end, whose max/min gain excursions are described by (1) and (2).

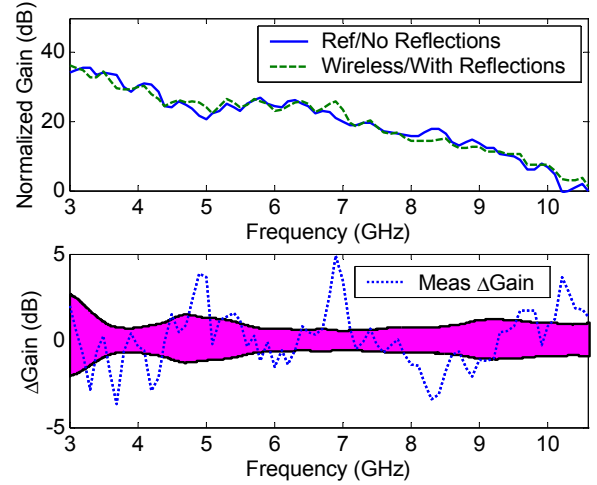


Figure 6. (a) Normalized transfer gain of reference w/o reflections and wireless w/ reflections (b) Theoretical and measured max/min gain excursions

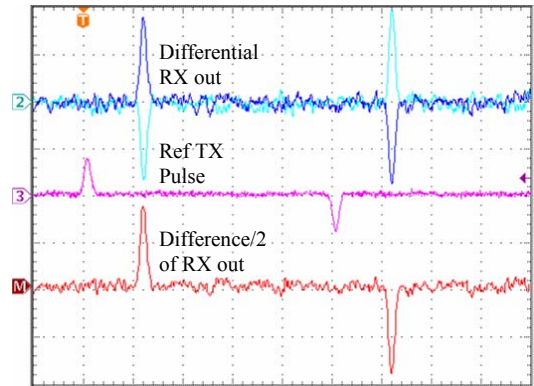


Figure 7. Oscilloscope plot of wirelessly received UWB pulses

The total channel losses seen in Fig. 6a exceed what is expected from channel propagation losses [5] and measured RFIC conversion gain variations over bandwidth. The additional losses are accounted for in the reduction of the UWB antenna's azimuthal radiation pattern at higher frequencies [6].

Fig. 6b uses measured values of  $S_{11, \text{Antenna}}$  and  $S_{11, \text{LNA}}$  to plot a patch of theoretical max/min gain excursions of the system. Superimposed on this patch is a plot of the difference between the reference transfer gain without reflections and wireless transfer gain with reflections found in Fig. 6a. The measured

gain difference falls outside the boundaries within a few dB through the band while residing mostly within the boundaries otherwise. Though the transfer gain from antenna to LNA may fluctuate, the input signal-to-noise ratio (SNR) does not, as the changes occur uniformly to both signal and noise.

An oscilloscope plot of a wirelessly received and down-converted pulse during coarse acquisition is shown in Fig. 7. The digital back-end in this system detects and compensates up to 100ns of channel impulse response [8].

The system in Fig. 1 is implemented with the horn and UWB antennas, packaged RFIC as the front-end, external baseband gain stages, a dual 500MS/s 8-bit ADC acquisition card, and a back-end receiver built in Matlab [8]. Fig. 8 shows the resulting BER plots that are obtained with multiple packets. Each packet contains a preamble with a Gold code to achieve coarse acquisition and channel estimation, followed by  $10^4$  bits of data being transmitted at 100Mbps.

For RX antenna powers greater than -76dBm, no errors in the packets were observed, so the desired  $10^{-5}$  BER performance is plotted, though it could conceivably be lower. The received power is verified by fixing the TX/RX antenna distances and measuring the power at the RX antenna with a spectrum analyzer. A BER of  $2.7 \times 10^{-3}$  is achieved at a low receiver sensitivity of -81dBm. To compare this received power vs. BER plot to a theoretical SNR vs. BER plot obtained in [9], a 500MHz  $kT$  noise power of -87dBm is assumed. SNR can be calculated by  $\text{dBm}_{\text{RX}} - 87 + \text{NF}$ . Fig. 8 matches to the SNR vs. BER plot within 2-3 dB.

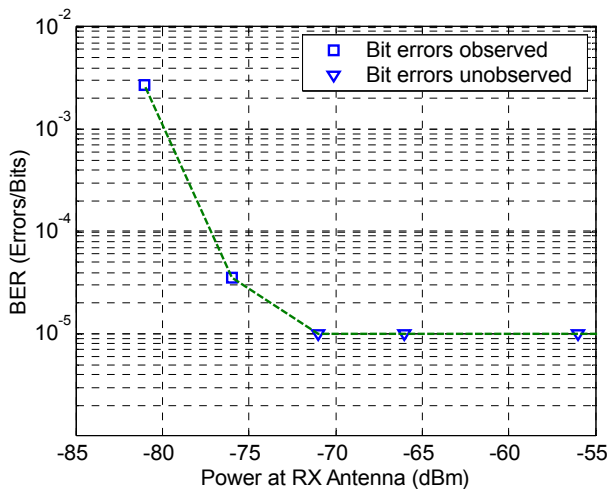


Figure 8. Wirelessly received power vs. BER at 6.85GHz channel

Table 2 shows the power breakdown of the front-end. The power consumption of the receiver can be further reduced and allocated more efficiently if the gain control is absorbed into the mixer and the biasing currents (~5mA total) are reduced. If the two LO gain chains are not included, the receiver consumes 40mW at a supply voltage of 1.8V. A summary of chip performance is reported in Table 3, and a die photo of the chip is shown in Fig. 9. The active area is 1mm x 2.3mm.

TABLE 2 – Power consumption at 1.8V

Block	Power (mW)
LNA	4.23
Buffer, S2D & notch	13.5
2 mixers and buffers	21.6
2 LO amplifiers	14.4
<b>Total</b>	<b>53.73</b>

TABLE 3 – Chip performance summary

Specification	Value from 3.1-10.6GHz
Conversion gain	39 to 29dB
Noise figure	3.3 to 5dB
Input P1dB	-46 to -36dBm
Notch filter attenuation	10dB
BER @ sensitivity	$2.7 \times 10^{-3}$ @ -81dBm
Process technology	0.18 $\mu$ m SiGe BiCMOS

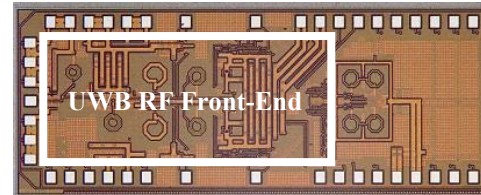


Figure 9. Die photo of chip

## Conclusions

A packaged 3.1-10.6GHz UWB RFIC front-end achieves a  $2.7 \times 10^{-3}$  BER at -81dBm sensitivity while consuming only 50mW. The system NF is 3.3-5dB from 3.1-10.6GHz. An un-matched low-power and low-noise UWB LNA is verified within a wireless receiver system. A switch-able RF notch filter embedded in an RF single-to-differential converter is shown to improve receiver performance and input DR.

## Acknowledgements

This research is sponsored by Hewlett-Packard under the HP/MIT Alliance and the National Science Foundation under contract ANI-0335256.

## References

- [1] Federal Communications Commission, *Ultra-wideband (UWB) first report and order*, Feb. 2002.
- [2] <http://www.ieee802.org/15/pub/TG3a.html>.
- [3] J. Lerdworatawee, W. Namgoong, "Low noise amplifier design for ultra-wideband radio," *2003 Proc. ISCAS*, May 2003.
- [4] A. Ismail, A. Abidi, "A 3.1 to 8.2GHz direct conversion receiver for MB-OFDM UWB communications," *2005 ISSCC Dig. Tech. Papers*, Feb. 2005.
- [5] S. Ghassemzadeh, et al., "UWB indoor path loss model for residential and commercial buildings," *2003 Trans. VTC*, Oct. 2003.
- [6] J. Powell, A. Chandrakasan, "Spiral slot patch antenna and circular disc monopole for ultra wideband communication," *2004 International Symposium on Antennas and Propagation*, Aug. 2004.
- [7] F. Lee, D. Wentzloff and A. Chandrakasan, "An ultra-wideband baseband front-end," *2004 Dig. RFIC Symp.*, June 2004.
- [8] R. Blazquez, A. Chandrakasan, "Architectures for energy-aware impulse UWB communication," *2005 ICASSP*, Mar. 2005.
- [9] R. Blazquez, et al, "Digital architecture for an ultra-wideband radio receiver," *2003 Trans. VTC*, Oct. 2003.